Alexander Kirst*, Anja Hellings-Kuß, Katharina Hagmann, Michael Dyck, Christopher Schlenk, and Julian Klodmann

A Novel End Effector for Telemanipulated Suturing in Robot-Assisted Laparoscopy

Abstract: Suturing is an integral part of surgery. Specialized instrumentation facilitates manual needle handling to support laparoscopic suturing tasks, e.g. uterine closure, in minimally invasive surgery. Current solutions for robot-assisted laparoscopy lack the possibility to integrate these instruments, making them suitable only for conventional laparoscopic surgery. This paper introduces a novel end effector design actuating a conventional suturing instrument. The end effector is integrated into the DLR MiroSurge system to facilitate telemanipulated suturing. The mechanical properties of the end effector are characterized and its feasibility for use in robot-assisted laparoscopy is demonstrated.

Keywords: robotic surgery, suturing, telemanipulation

1 Introduction

Robotic assistance and telemanipulation play an increasingly important role in laparoscopy. Restoration of hand-eye coordination and increased dexterity through additional degrees of freedom (DoFs) enhance the physicians' capabilities during surgery. However, suturing tasks are still physically demanding and time-consuming. The main reason for this, is the difficulty to grasp the needle in an appropriate pose to allow for the next step. To guarantee deterministic needle pose with respect to the robotic instrument (and to facilitate higher levels of autonomy during suturing tasks in the future), this paper presents a novel end effector (EE) for robot-assisted suturing in laparoscopy (see Fig. 1).

Our contributions are:

$C1$ Design and development of an EE actuating all DoFs of an integrated conventional suturing instrument.

$C2$ Integration of the EE into the DLR MiroSurge telemanipulation system to facilitate needle handling.

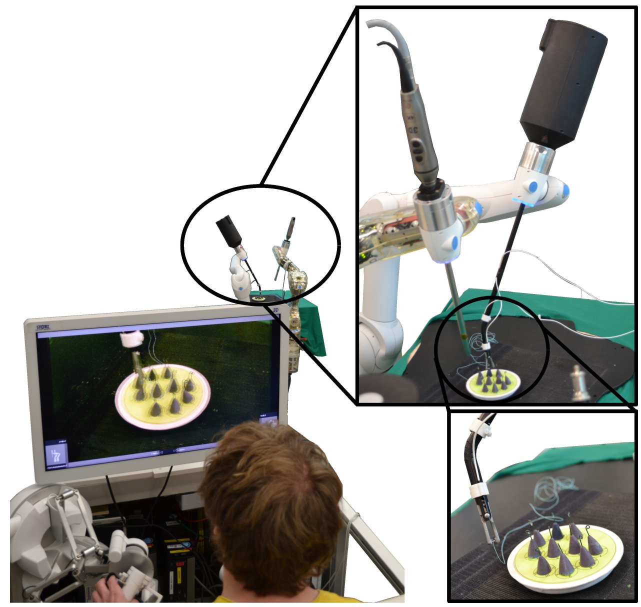

Fig. 1: Telemanipulated suturing on a standardized hook training task utilizing the presented end effector (EE), fully integrated into the DLR MiroSurge system. Foreground: surgeon console; background: two DLR MIRO arms, carrying the EE or the stereo endoscope, respectively.

2 State of the Art

In both, industry and research, various mechatronic approaches towards enhancing surgical suturing exist. They can be divided into two categories, i.e. hand-held and robotic. Several specialized hand-held instruments for conventional laparoscopy are on the market and commercially available, such as the Endo Stitch™ and SILS™ Stitch (Medtronic plc, formerly Covidien), or the Endo360° (EndoRevolution).

The STAR system [1], [2] by Leonard et al. introduces an EE, consisting of an actuated hand-held instrument Endo360° to be used as robotic EE on a KUKA LWR robot arm. Another example of an EE for robotic suturing is the EndoSew system [3], which introduced a novel robotic EE designed from scratch. Besides these two mechatronic approaches, sensor- and control-related solutions are also being pursued to make suturing more convenient, e.g., the SNAP system from Sen et al. [4].

***Corresponding author: Alexander Kirst,** Institute for Robotics and Mechatronics, DLR, Münchener Straße 20, 82234 Weßling, Germany, e-mail: Alexander.Kirst@dlr.de
Anja Hellings-Kuß, Katharina Hagmann, Michael Dyck, Christopher Schlenk, Julian Klodmann, Institute for Robotics and Mechatronics, DLR, Münchener Straße 20, 82234 Weßling, Germany
Michael Dyck, TUM School of Computation, Information and Technology, Technical University of Munich

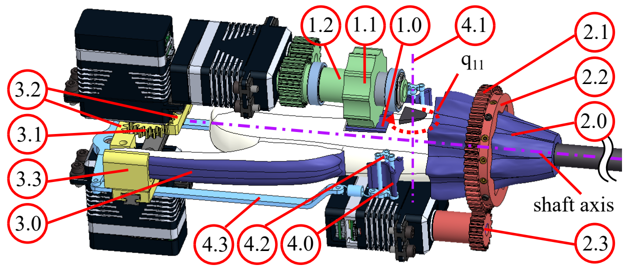

Fig. 2: CAD model of the actuating mechanisms of the EE, see Fig. 3 for the distal part, including the generalized coordinates q_8, q_9, q_{10}.

3 Material and Methods

This chapter presents the materials used (Sec. 3.1), the design of the drive unit (Sec. 3.2) and its kinematics (Sec. 3.3).

3.1 Material

The core element of the EE presented in this work is the commercially available suturing instrument SILS™ Stitch (Medtronic plc, formerly Covidien) [7]. To facilitate suturing in single-port laparoscopy, this instrument provides two additional DoFs - bending and rotation - at the tooltip (see q_8 and q_9 in Fig. 3). The fixation of the needle in either one of the two jaws of the gripper ensures a deterministic needle pose at all times.

In-house developed motors are used to actuate the DoFs of the EE. These motors have a no-load speed of 17 rad/s and a stall torque of 1.9 Nm. The majority of the mechanical parts inside the EE, as well as the casing, are 3D-printed with multi jet fusion. The EE fits the flange of the seven DoF lightweight robotic arm, DLR MIRO [5]. The DLR MiroSurge system [6] serves as telemanipulation system for the integrated EE.

3.2 Design of the Drive Unit

The SILS™ Stitch incorporates four DoFs, described as the four generalized coordinates $\mathbf{q} = [q_8, q_9, q_{10}, q_{11}]^T$, to perform suturing, which are shown in Fig. 2 and Fig. 3: (1) bending of the tip (q_8), (2) rotation of the tip (q_9), (3) opening and closing of the gripper (q_{10}), and (4) needle transfer between the jaws (q_{11}). The instrument wasn't disassembled to allow an easy exchange of the disposable instrument without much effort while changing. Fig. 2 depicts the CAD model of the EE (without housing) and numbered parts, which are referred to in the following.

Bending of the tip (q_8) requires rotating a wheel (1.0) on the instrument. As this wheel is designed for rotation by hand and does not have an involute gearing, a dedicated flexible gear (1.1) was printed using flexible filament (Cheetah TPU, NinjaTek) with small wall thickness and little infill. The flexible gear is pushed into the instrument gear, ensuring torque transmission, based on force and form fit. It is fastened on a mechanical shaft (1.2).

Rotating the tip (q_9) is enabled by a cone-shaped wheel at the origin of the instrument shaft (2.0). A gear (2.1) is glued to its formfitting part (2.2), which is fixated by radial screws on part (2.0). An additional gear (2.3) connects the servo motor.

Opening and closing of the gripper (q_{10}) is achieved by pushing a spring-loaded handle (3.0) at the instrument base. To realize this motion with a rotational servo motor, a parallel mechanism was designed. A gear (3.1) attached to the motor is placed between two gear racks (3.2). These racks sliding along a linear rail integrate the negative counterparts (3.3) of the handle claws at their distal end, enabling to squeeze the claws. Thus, rotational motion of the motor results in motion of the two gear-racks in opposite directions, resulting in opening or closing of the handle.

The needle transfer mechanism (q_{11}) of the instrument works through a lever (4.0), that can be rotated around a fixed axis (4.1) inside the instrument body. Due to the confined space, the motor actuating this DoF is placed in the proximal part of the EE. A parallel mechanism changes the rotary motor motion to the translation of the rods (4.2) in opposite directions. The rods are connected to the two extremities of the lever (4.0) by a cage (4.3). Thus, their translational motion results in the rotation of the lever.

The mapping of the generalized coordinates and the motor angles was assumed linear, given by the transmissions of the gears.

3.3 Kinematics

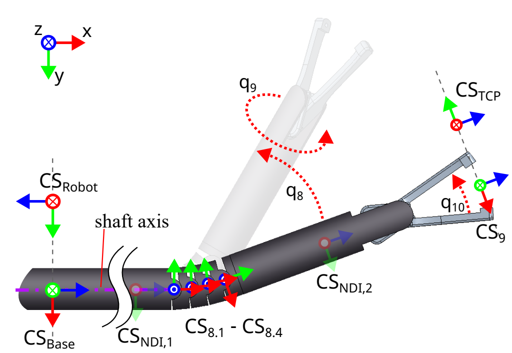

Fig. 3: Coordinate systems (CS) and generalized coordinates q_8, q_9, q_{10} of the EE, see Fig. 2 for the proximal part and q_{11}.

The continuous bending kinematics at the tip (q_8) of the instrument can be described by a rotation around four parallel axes arranged on a circle with variable radius, where a secant line intersects with the origins of $CS_{8.1}$ and $CS_{8.4}$. The CS in Fig. 3 are described by the Denavit-Hartenberg (DH) notation,

Tab. 1: DH parameters of the EE

i	a_{i-1}	α_{i-1}	d_i	Θ_i
8_1	0	$\frac{\pi}{2}$	$410\,mm$	$\frac{\pi}{2}+\frac{q_8}{6}$
8_2	$4\,mm$	0	0	$\frac{q_8}{3}$
8_3	$4\,mm$	0	0	$\frac{q_8}{3}$
8_4	$4\,mm$	0	0	$-\frac{\pi}{2}+\frac{q_8}{6}$
9	0	$-\frac{\pi}{2}$	$53\,mm$	q_9

their corresponding parameters are in Tab 1. Tab. 1 shows the set of DH parameters, with $i = 8_1...8_4$ referring to the four parallel axes. The constant homogeneous transformation matrices ${}^{Robot}T_{Base}$ and ${}^{9}T_{TCP}$ complete the kinematics chain of the instrument.

We refer to the seven DoFs of the MIRO robot arm as q_1 - q_7, and complete the kinematics chain with the EE through its four DoF q_8 - q_{11}.

The joint limits of q_8 are 6° and 70°, for q_9 they are -180° and 180°. The value for q_{10} ranges from 0 to 1, with 0 being a closed, and 1 an open gripper. The values for q_{11} range from -1 to 1, corresponding to the needle position in the left or the right jaw, respectively.

For modeling the inverse kinematics of the instrument, a differential inverse kinematics based on the forward kinematics Jacobian was implemented. The inverse kinematics of the entire MiroSurge system is given in [8].

4 Results and Discussion

4.1 Verification

To verify the performance of the EE, the absolute accuracy (Acc), repeatability (Reap), and multi-directional repeatability (mReap), or rather hysteresis, of the two positioning DoFs q_8 (bending) and q_9 (rotation) are evaluated. Therefore, the instrument is placed above a NDI® Aurora electromagnetic tracking device with two six DoF NDI® sensors placed at the shaft and the tip of the instrument, respectively (cmp. Fig. 3, $CS_{NDI,\{1,2\}}$). All motors were outside the measuring field, to avoid disturbances of the electro-magnetic field by the electronics of the motors. For bending of the instrument tip, q_8 is commanded along a cyclic trajectory between 10° and 65°. Static positions are held in a step size of 5°. This trajectory is repeated 30 times. Accordingly, a cyclic trajectory is conducted for the rotation of the tooltip (q_9) with a range of +/- 180° and a step size of 10°, repeated 10 times. Acc, Reap, and mReap are computed, adjusting the formulas of the standard ISO 9283 for a single DoF.

Fig. 4 shows the error between desired and actual angle for both DoFs. The gray curves show the error for each individual trajectory, with the red curve representing the average over all trajectories.

The accuracy (Acc) is calculated as the mean of the distance between the red curve and the 0° line for every measured angle, being Acc = 10.11° for q_8 and Acc = 17.62° for q_9. Furthermore, the height of the grey area representing the results of each individual trajectory is an indicator for the repeatability (Reap, see Tab. 2) of both DoFs. Finally, the difference in error for the two motion directions in each cyclic trajectory - the vertical gap between the two error values for a single desired angle - implies hysteresis behavior of both DoFs. The corresponding maxima of this gap (mReap) are given in Tab. 2.

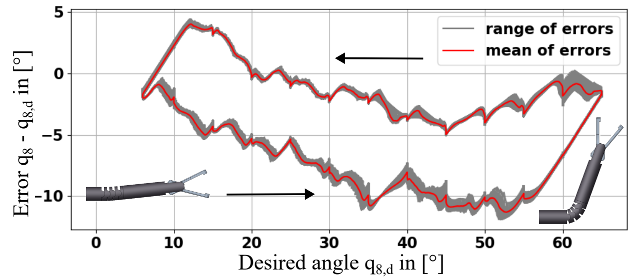

(a) Bending of the instrument tip

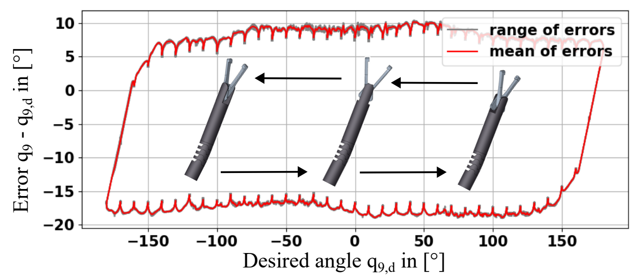

(b) Rotation of the instrument tip

Fig. 4: Verification of the EE performance

Tab. 2: Performance metrics

Quality measures	q_8	q_9
Acc	10.11°	17.62°
Reap	0.60°	0.35°
mReap	5.34°	23.75°

4.2 Suturing

Finally, we evaluate the proof of concept of our EE for telemanipulated suturing on a trainingspad (S Hooks Pod No.4025, The Chamberlain Group, [9]). This pad was modified to spread hooks with a diameter of 2 mm to allow the needle to fit through. The goal is to guide the needle through every hook of the pad. The task is performed two times by two different non-expert participants. The position of the tooltip is measured with the NDI system and its trajectory is visualized relative to the pad in Fig. 5, upper right. Exemplary, in the lower half of Fig. 5 five images show the needle handling on one hook. The lower part of Fig. 5 depicts the values of q_{10} and q_{11} for this exemplary needle stitching and transfer subtask of suturing.

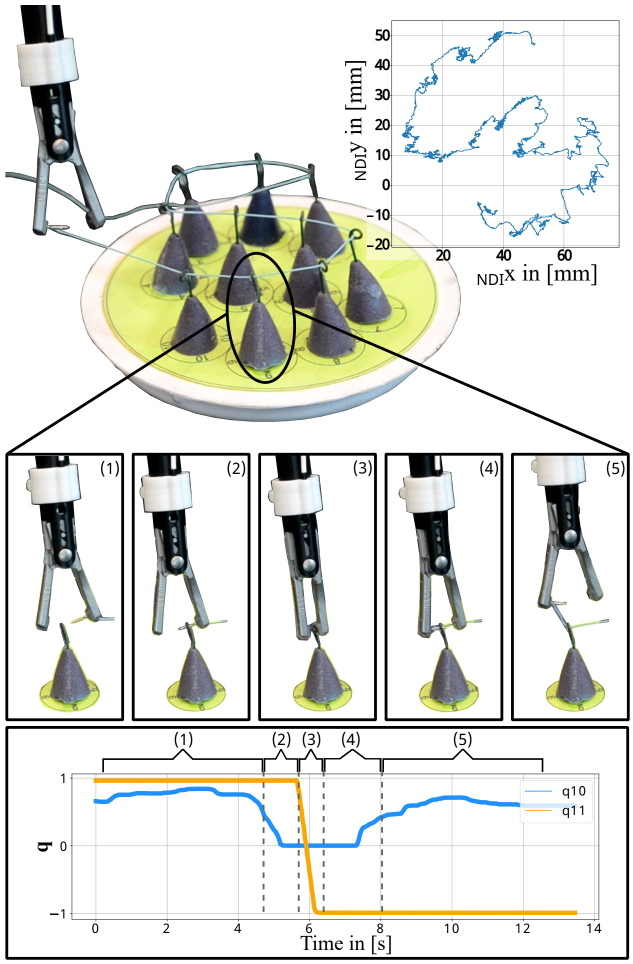

Fig. 5: Overview of the suturing task with the phases of one needle stitching and transfer subtask. (1) the needle is in the right jaw and the tip is approaching the hook (2) closing of the jaws around the hook, (3) the needle is transferred to the other jaw, (4) the jaws are opening and the needle is in the left jaw, (5) the EE moves away from the hook, but the thread runs through the hook, upper right: position of the tooltip in NDI coordinates

4.3 Discussion

The verification shows high repeatability (Reap < 1°), but a limited accuracy of the presented EE. This can be explained with a deterministic, but nonlinear behavior of the mapping between motors and EE DoFs and backlash in the gearing. Additionally, the backlash in the DoFs of the instrument itself results in the observed hysteresis. Depending on the back drivability of the instrument, either model-based backlash compensation methods or feedback control of the instrument pose, e.g. based on optical tracking, could improve the performance.

Finally, the second experiment demonstrated the suitability of our EE for telemanipulated suturing in the exemplary suturing task.

5 Conclusion and Outlook

This work presented a novel EE for telemanipulated suturing in robot-assisted laparoscopy. Future work will involve improvement of the actuation of the EE, e.g. model-based backlash compensation methods, as well as integration and utilization of sensory information, e.g. optical instrument tracking [10], for feedback control of the Cartesian instruments pose. Experiments with the EE during more realistic suturing tasks including interaction forces, will give further insight on the performance of the instrument.

Author Statement

The authors have no conflict of interest to disclose.

References

[1] Leonard S, Wu KL, Kim Y, Krieger A and Kim PCW. Smart Tissue Anastomosis Robot (STAR): A Vision-Guided Robotics System for Laparoscopic Suturing. IEEE Transactions on Biomedical Engineering; 61:1305-1317.

[2] Leonard S, Shademan A, Kim Y, Krieger A, Kim PCW. Smart Tissue Anastomosis Robot (STAR): Accuracy evaluation for supervisory suturing using near-infrared fluorescent markers. IEEE International Conference on Robotics and Automation 2014:1889-1894.

[3] Roth B, Birkhäuser FD, Thalmann GN, Zehnder P. Novel prototype sewing device, EndoSew, for minimally invasive surgery: an extracorporeal ileal conduit construction pilot study in 10 patients. BJUI International 2013.

[4] Sen S, Garg A, Gealy DV, McKinley S, Jen Y, Goldberg K. Automating multi-throw multilateral surgical suturing with a mechanical needle guide and sequential convex optimization IEEE International Conference on Robotics and Automation 2016:4178-4185.

[5] Hagn U, Nickl M, Jörg S, Passig G, Bahls T, Nothhelfer A et al. The DLR MIRO: a versatile lightweight robot for surgical applications. Industrial Robot: An International Journal 2008;35(4):324-336.

[6] Hagn U, Konietschke R, Tobergte A, Nickl M, Jörg S, Kübler B et al. DLR MiroSurge - A Versatile System for Research in Endoscopic Telesurgery. International Journal of Computer Assisted Radiology and Surgery 2009:183-193.

[7] Covidien Launches SILS™ Stitch Suturing Device for Advanced Laparoscopic Surgery, https://www.youtube.com/watch?v=GmKkAx5fS44, last accessed at 21.06.2023

[8] Tobergte A, Konietschke R, Hirzinger G. Planning and real time control of a minimally invasive robotic surgery system. ICRA Proceedings 2009.

[9] S Hooks Pod No. 4025, https://www.thecgroup.com/product/robotic-s-hook-pod-4025/, last accessed at 25.06.2023

[10] Stoiber M, Pfanne M, Strobl KH, Triebel R, Albu-Schäffer A. SRT3D: A sparse region-based 3D object tracking approach for the real world. International Journal of Computer Vision 2022;130.4:1008-1030.